About 2D Cavity Resonance

May 12, 2026

July 21, 2026 Revised

Takuya Yabu(takuya.yabu@live.jp)

Abstract

Research on automobile whistling and suction sounds has been conducted in the past. For cavity resonance, a type of whistling sound, the cavity resonance frequency has been determined using Rossiter's empirical formula. Therefore, we limited our study to the two-dimensional case and clarified the physical phenomena that arise by solving a set of partial differential equations that explain the phenomenon. As a result, the horizontal resonance frequency was found to become proportional to the speed of sound as the mainstream velocity increased, and the resonance frequency of the cavity space was also determined. Finally, we discussed the conditions under which resonance increases. Finally, we were able to confirm the conditions under which resonance increases through numerical calculations.

Nomenclature

L_H: Maximum hole length

ρ, c: Air density and air sound speed

ω: Angular frequency

f_x: Frequency obtained from Rossiter's formula

f_{xr}, f_y: x-direction resonance frequency and y-direction resonance frequency

k: Wavenumber

t: Time

j: Imaginary unit

U, U_{vx}: Mainstream air velocity and vortex (vorticity) velocity

κ: Ratio of vortex (vorticity) velocity to mainstream air velocity

$\hat{G}_v(s)$: Fluid-driven gain

ϕ_v: Phase lag component of the fluid-driven gain

θ_{2D}: Phase lag component caused by the cavity space

M: Mach number

ζ: Vorticity

α: Efficiency of conversion from vorticity to sound pressure (dimension: L^2)

β: Efficiency of conversion from sound pressure to vorticity (dimension: $\mathrm{L}^2\mathrm{M}^{-1}\mathrm{T}^1$)

$\delta(x)$: Dirac delta function

$\delta'(x)$: Differential of Dirac delta function

$H(x)$: Heaviside step function

s: Complex number

L_y: Depth of the box

$u(x,y,t), v(x,y,t)$: Velocity in the x direction and velocity in the y direction

1. Introduction

In the past, research has been conducted on the whistling and suction sounds of automobiles (Calvo, Diaz, & San Roman, 2005) (Chien-Hsiung, Lung-Ming , Chang-Hsien , Yen-Loung , & Jik-Chang , 2009) (George, 1990) (Jagtiani, 1972) (Jung & Oh, 1995) (Münder & Carbon, 2022) (Oettle & Sims-Williams, 2017) (Qatu, Abdelhamid, Pang, & Sheng, 2009) (Wang, Chen, & Zhang, 2021) (Zhang, Meng, Li, & Zheng, 2022). Cavity resonance is a type of whistling sound. In cavity resonance, the cavity resonance frequency has traditionally been determined using Rossiter formula, an empirical formula. Therefore, for cavity resonance in the two-dimensional case, we will clarify the physical phenomena that arise by solving the set of partial differential equations that explain the phenomenon. Finally, we will examine the conditions under which resonance increases in numerical calculations.

These will be discussed below.

2. About 2D Cavity Resonance

2.1. Vorticity Movement Equation

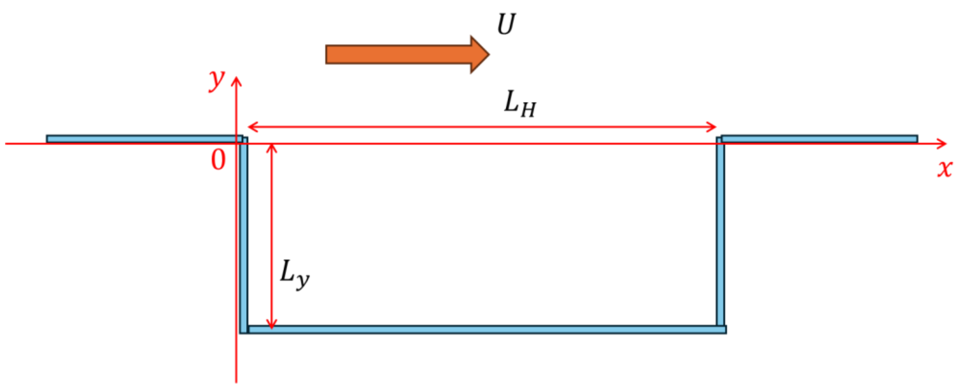

Fig. 1 2-Dimensional Box with Hole

Fig. 1 shows a box with a hole. Here, the conventional definitions of cavity resonance and cavity resonance frequency are given below.

Definition :

When air is flowing at velocity U and there is a hole, a vortex moves from the upstream end to the downstream end of the hole. This vortex collides with the downstream end, generating sound. This generated sound then moves from the downstream end to the upstream end. Sound is a change accompanied by particle velocity, and this particle velocity then collides with the upstream end, generating another vortex. This series of phenomena is defined as "cavity resonance." Furthermore, the reciprocal of the time from when a vortex moves and generates sound until another vortex is generated is defined as the "cavity resonance frequency."

Based on this definition, we derive the differential equation representing cavity resonance, limited to two dimension. First, the movement equation of vorticity $\zeta(x, y, t)$ is expressed by the following equation. However, the viscosity term is ignored.

$$\frac{\partial \zeta}{\partial t} + U_{vx} \frac{\partial \zeta}{\partial x} = 0 \tag{1}$$

2.2. Powell's Equation

Next, we will find the relationship between sound pressure and vorticity.

Powell's equation is the relationship between sound pressure and vorticity. Expressed in two dimension, Powell's equation is given by the following:

$$\frac{1}{c^2}\frac{\partial^2 p}{\partial t^2} - \left(\frac{\partial^2 p}{\partial x^2} + \frac{\partial^2 p}{\partial y^2}\right) = \alpha\rho[\zeta(L_H, 0, t)u(L_H, 0, t)\delta'(x - L_H)\delta(y) - \zeta(L_H, 0, t)v(L_H, 0, t)\delta(x - L_H)\delta'(y)] \tag{2}$$

2.3. Initial Conditions

The initial condition for the velocity in the x-direction is given below:

$$u(x, y \geq 0, 0) = U \tag{3}$$

The initial condition for the velocity in the y-direction is given below:

$$v(x, y, 0) = 0 \tag{4}$$

The initial condition for the sound pressure is given below:

$$p(x, y, 0) = 0 \tag{5}$$

The initial condition for the time derivative of the sound pressure is given below:

$$\left.\frac{\partial p}{\partial t}\right|_{t=0} = 0 \tag{6}$$

2.4. Boundary Conditions

We need to find the boundary conditions under which the velocity of the returned particles changes to vorticity. These are given by the following equation:

$$\zeta(0,0.t) = -\beta_x \left.\frac{\partial p}{\partial x}\right|_{(x=0,y=0,t=t)} \tag{7}$$

Furthermore, assuming that sound pressure is completely reflected at the bottom of the box and becomes zero at the open end, the following conditions hold true.

$$\left.\frac{\partial p}{\partial x}\right|_{y=-L_y} = 0 \tag{8}$$

Furthermore, assuming that the sound pressure is completely reflected by the left and right walls, the following conditions hold true.

$$\left.\frac{\partial p}{\partial x}\right|_{x=0,-L_y\leq y\leq 0} = 0 \tag{9}$$

$$\left.\frac{\partial p}{\partial x}\right|_{x=L_H,-L_y\leq y\leq 0} = 0 \tag{10}$$

3. Resonance Frequency of a Two-Dimensional Cavity Resonance

3.1. Solution to the Vorticity Transfer Equation

We derive the resonance frequency of a two-dimensional cavity resonance. First, we solve equation (1). The solution when the boundary condition is $\zeta(0,t)$ is given by the following equation:

$$\zeta(x,y,t) = \zeta\left(0,0,t-\frac{x}{U_{vx}}\right) \tag{11}$$

3.2. Sound Pressure Equation Using Green's Function Derived from Powell's Equation

Next, we solve Powell's equation (2). This can be obtained using the Green's function in the following form. First, the Green's function is given by the following equation.

$$G(x,y,t|x',y',\tau) = \frac{c}{2\pi}\frac{H(c(t-\tau)-r')}{\sqrt{c^2(t-\tau)^2-r'^2}} \tag{12}$$

Here, the following equation holds true.

$$r' = \sqrt{(x-x')^2+(y-y')^2} \tag{13}$$

From equations (2) and (12), the following equation is obtained.

$$p(x,y,t) = -\frac{\alpha\rho c}{2\pi}\sum_{n=-\infty}^{\infty}\int_0^{t-\frac{r_{n,1}}{c}}\frac{\Phi_{n,1}(\tau)}{\sqrt{c^2(t-\tau)^2 - r_{n,1}^2}}d\tau$$

$$+\frac{\alpha\rho c}{2\pi}\sum_{n=-\infty}^{\infty}\int_0^{t-\frac{r_{n,2}}{c}}\frac{\Phi_{n,2}(\tau)}{\sqrt{c^2(t-\tau)^2 - r_{n,2}^2}}d\tau \tag{14}$$

Here, the following equation holds true.

$$\Phi_{n,1}(\tau) = \frac{(u(L_H,0,\tau)\cdot(x-(2n+1)L_H) - (-1)^n\cdot v(L_H,0\,,\tau)\cdot y)\zeta(L_H,0,\tau)}{c^2(t-\tau)^2 - r_{n,1}^2} \tag{15}$$

$$r_{n,1} = \sqrt{(x-(2n+1)L_H)^2 + y^2} \tag{16}$$

$$\Phi_{n,2}(\tau) = \frac{\left(u(L_H,0,\tau)\cdot(x-(2n+1)L_H) - (-1)^n\cdot v(L_H,0\,,\tau)\cdot\left(y+2L_y\right)\right)\zeta(L_H,0,\tau)}{c^2(t-\tau)^2 - r_{n,2}^2} \tag{17}$$

$$r_{n,2} = \sqrt{(x-(2n+1)L_H)^2 + \left(y+2L_y\right)^2} \tag{18}$$

3.3. Stability Condition and Frequency in the Mainstream Air Velocity Direction and Cavity Resonance Frequency

We consider the stability conditions for the solution obtained in Equation (14). Applying the Laplace transform to both sides yields the following equation, where we set $u(L_H,0,s) = U$. To examine stability, we assume $\zeta(L_H,0,s) = \zeta_0 e^{st}$ and $v(L_H,0,s) = v_0 e^{st}$. Additionally, $K_0(x)$ denotes the modified Bessel function of the second kind.

$$p(x,y,s) = -\frac{\alpha\rho c}{2\pi}\sum_{n=-\infty}^{\infty}(U(x-(2n+1)L_H) - (-1)^n v_0 y e^{st})\zeta_0 e^{st}\cdot\frac{1}{c}K_0\left(\frac{r_{n,1}}{c}s\right)$$

$$+\frac{\alpha\rho c}{2\pi}\sum_{n=-\infty}^{\infty}\left(U(x-(2n+1)L_H) - (-1)^n v_0\left(y+2L_y\right)e^{st}\right)\zeta_0 e^{st}\cdot\frac{1}{c}K_0\left(\frac{r_{n,2}}{c}s\right) \tag{19}$$

Here, since linear theory is employed, the term e^{2st} can be neglected as an infinitesimal quantity. Consequently, the following equation is obtained:

$$p(x,y,s) = -\frac{\alpha\rho U\zeta_0}{2\pi}\sum_{n=-\infty}^{\infty}(x-(2n+1)L_H)K_0\left(\frac{r_{n,1}}{c}s\right)$$

$$+\frac{\alpha\rho U\zeta_0}{2\pi}\sum_{n=-\infty}^{\infty}(x-(2n+1)L_H)K_0\left(\frac{r_{n,2}}{c}s\right) \tag{20}$$

Given that the summation of $(2n+1)$ from $n=-\infty$ to ∞ results in zero, the following equation is obtained:

$$p(x,y,s) = -\frac{\alpha\rho U\zeta_0 x}{2\pi}e^{st}\sum_{n=-\infty}^{\infty}\left(K_0\left(\frac{r_{n,1}}{c}s\right) - K_0\left(\frac{r_{n,2}}{c}s\right)\right) \tag{21}$$

Considering that self-excited oscillations arise when a vortex generated at the upstream edge of the cavity—relative to the mainstream flow—strikes the downstream edge to produce sound, and that sound then travels back from the downstream edge to the upstream edge, the following equation is obtained. Here, we set $p(x, y, s) = p_0 e^{st}$.

$$p_0 e^{st} = -\frac{\alpha\rho U\zeta_0 x}{2\pi} e^{st} e^{-s\left(\frac{L_H}{U_{vx}}+\frac{L_H}{c}\right)} \sum_{n=-\infty}^{\infty} \left(K_0\left(\frac{r_{n,1}}{c}s\right) - K_0\left(\frac{r_{n,2}}{c}s\right)\right) \tag{22}$$

Therefore, letting $\hat{G}_v(s)$ represent the fluid-driven gain, the characteristic equation is given by the following expression:

$$1 - \hat{G}_v(s)\left(-\frac{\alpha\rho U\zeta_0 x}{2\pi} \sum_{n=-\infty}^{\infty} \left(K_0\left(\frac{r_{n,1}}{c}s\right) - K_0\left(\frac{r_{n,2}}{c}s\right)\right)\right) e^{-s\left(\frac{L_H}{U_{vx}}+\frac{L_H}{c}\right)} = 0 \tag{23}$$

Consider the frequency f_x in the mainstream air direction. In this case, the following equation holds based on Equation (23). Here, ϕ_v represents the phase lag component of the fluid-driven gain, and θ_{2D} represents the phase lag component caused by the cavity space.

$$-\phi_v - \theta_{2D} - \omega\left(\frac{L_H}{U_{vx}} + \frac{L_H}{c}\right) = -2\pi n$$

$$2\pi\left(n - \frac{\phi_v + \theta_{2D}}{2\pi}\right) = 2\pi f_x\left(\frac{L_H}{U_{vx}} + \frac{L_H}{c}\right)$$

$$f_x = \frac{\left(n_x - \frac{\phi_v + \theta_{2D}}{2\pi}\right)}{\frac{L_H}{U_{vx}} + \frac{L_H}{c}} \tag{24}$$

Finally, by setting $U_{vx} = \kappa U$, the following equation is obtained. Conventionally, a value of 0.25 or close to it has been used for the phase lag in Rossiter's formula. Based on stability conditions, however, it was possible to derive from Equation (23) that $\frac{\phi_v+\theta_{2D}}{2\pi}$ should be used as the phase lag in Rossiter's formula.

$$f_x = \frac{U}{L_H}\frac{\left(n_x - \frac{\phi_v + \theta_{2D}}{2\pi}\right)}{\left(\frac{1}{\kappa} + \frac{U}{c}\right)} \tag{25}$$

Next, applying the Poisson summation formula to the modified Bessel function of the second kind in Equation (23) yields the following equation:

$$1 - \hat{G}_v(s)\left(-\frac{\alpha\rho U\zeta_0 x}{2\pi} \sum_{n=-\infty}^{\infty} \left(\frac{e^{-s\frac{|y|}{c}} - e^{-s\frac{|y+2L_y|}{c}}}{s^2 + \left(\frac{n\pi c}{L_H}\right)^2}\right) \cos\left(\frac{n\pi c}{L_H}\right)\right) e^{-s\left(\frac{L_H}{U_{vx}}+\frac{L_H}{c}\right)} = 0 \tag{26}$$

From this equation, substituting $s = j\omega$ to analyze the stability conditions reveals that the expression diverges to infinity when:

$$\omega = \frac{n\pi c}{L_H} \tag{27}$$

Here, substituting $\omega = 2\pi f_{xr}$ and $n = n_{xr}$ yields the following equation:

$$f_{xr} = \frac{n_{xr} c}{2L_H} \tag{28}$$

At this frequency, cavity resonance—a form of self-excited oscillation—occurs. This frequency corresponds to the resonance frequency in the x-direction.

Conversely, based on Equation (26), the resonance frequency in the y-direction given by the following equation does not occur:

$$f_y = \frac{\left(2n_y - 1\right) \cdot c}{4L_y} \tag{29}$$

Unlike the resonance frequency of a standard enclosed space, a frequency f_x in the mainstream air velocity direction is generated first. When this matches the resonance frequency in the x-axis direction, a lock-in phenomenon occurs, resulting in a loud sound.

3.4. Insights from the Frequency in the Mainstream Air Velocity Direction

By further transforming the frequency in the mainstream sir velocity direction (Equation (25)) and taking the limit as $U \to \infty$, the following equation is obtained:

$$f_x = \frac{U}{L_H} \frac{\left(n_x - \frac{\phi}{2\pi}\right)}{\left(\frac{1}{\kappa} + \frac{U}{c}\right)} \to \frac{\left(n_x - \frac{\phi}{2\pi}\right)}{L_H} c \tag{30}$$

In other words, as the mainstream velocity increases, the frequency in the mainstream direction becomes proportional to the speed of sound.

3.5. Sound Pressure at a Position Outside the Sound Source ($x \geq L_H$)

We will now discuss the sound pressure at a position outside the sound source ($x \geq L_H$). As before, it can be calculated using the following equation.

$$p(x, y, t) = \frac{\alpha\rho c}{2\pi} \int_0^{t-\frac{r}{c}} \frac{\left[\frac{1}{c}\frac{\partial}{\partial\tau}\frac{\Phi_{2D}(\tau)}{r} - \frac{1}{r^2}\Phi_{2D}(\tau)\right]}{\sqrt{c^2(t-\tau)^2 - r^2}} d\tau \tag{31}$$

Here, the following equation holds true.

$$\Phi_{2D}(\tau) = (u(L_H, 0, \tau) \cdot (x - L_H) - v(L_H, 0, \tau) \cdot y)\zeta(L_H, 0, \tau) \tag{32}$$

$$r = \sqrt{(x - L_H)^2 + y^2} \tag{33}$$

4. Numerical Calculations

The results were confirmed by numerical calculation. The values used are shown in Table 1 below.

Furthermore, for $\frac{\partial p}{\partial x}$ and $v(L_H, 0, t)$, it was assumed that vortices were continuously generated at the upstream end at a Rossiter formula primary frequency of 9.6 (Hz), and that this vortex mass was continuously excited at the downstream end as $v(L_H, 0, t)$ at the same Rossiter formula primary frequency of 9.6 (Hz). Therefore, the following equation is continuously used during the numerical calculation. Here, $f_{x,1}$ is the Rossiter formula primary frequency of 9.6 (Hz).

$$\frac{\partial p}{\partial x} = \sin(2\pi f_{x,1} t) \tag{34}$$

$$v(L_H, 0\,, t) = \frac{1}{2}\sin(2\pi f_{x,1} t) \tag{35}$$

Table 1 Parameter and Value

Parameter	Value
ρ	1.225(kg/m^3)
c	340.0(m/s)
U	34.0(m/s)
κ	0.6
α	1(m^2)
β_x	0.01(m^{2}s/kg)
$\phi_v + \theta_{2D}$	$\frac{\pi}{2}$
L_H	1.5(m)
L_y	0.7(m)

The numerical calculation results are shown in Fig. 2. The observation position was $(x, y) = (0.01, 0.01)$ near the origin. The top graph shows the time-series waveform of sound pressure, and the bottom graph shows the frequency characteristics of sound pressure.

Looking at the time-series waveform of sound pressure in Fig. 2, we can see that waveforms from various sound sources are combined and gradually increase in size as self-excited oscillations. In other words, it is clear that cavity resonance is self-excited.

Next, examining the frequency characteristics of the sound pressure shown in Fig. 2, a peak corresponding to the first-order frequency of Rossiter's formula (f_x) appears at 9.6 (Hz). Additionally, peaks are observed at the resonance frequency f_{xr} (113.3 (Hz)) and its integer multiples, indicating the presence of resonance frequencies in the x-direction. This is because the sound energy cannot escape into other dimensions; instead, it flows into the resonant frequencies of each f_x order—where peaks would not normally occur—thereby generating peaks. Conversely, for f_y, no oscillation is excited, even at frequencies close to the f_x resonance frequency. This finding supports the discussion regarding Equation (26).

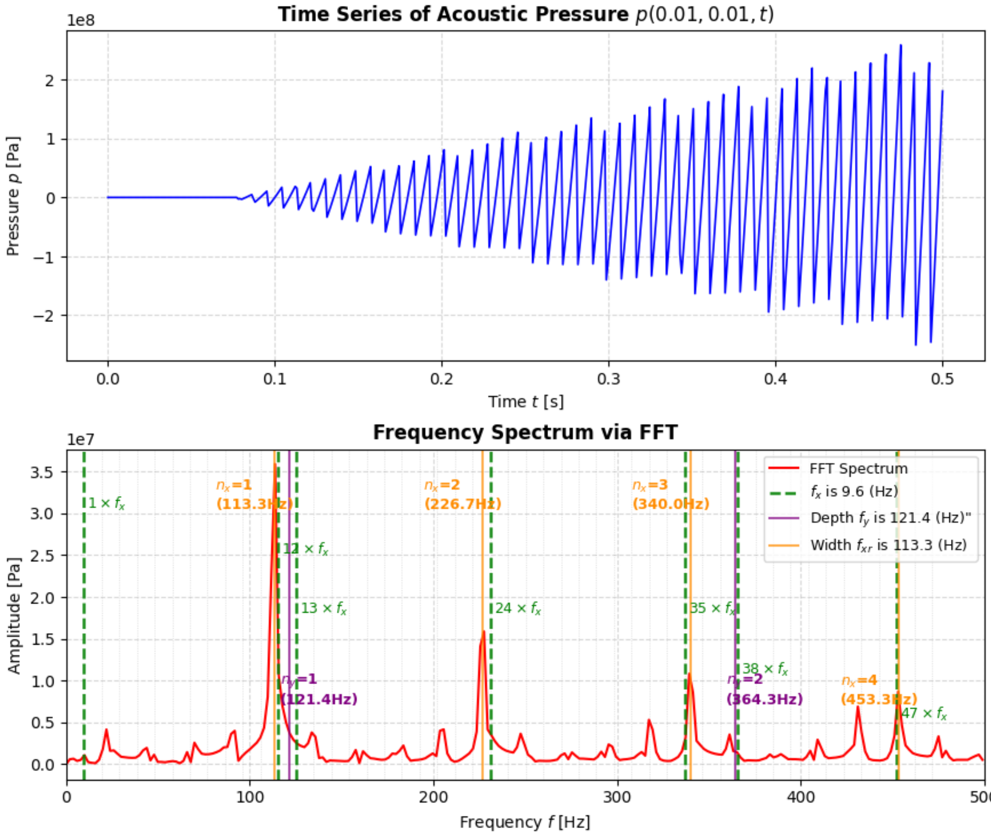

Fig. 2 Numerical Calculation Results

Next, we calculate the sound pressure for $x \geq L_H$. The results are shown in Fig. 3. The observation position was $(x, y) = (2.0, 0.5)$. The top graph shows the time-series waveform of the sound pressure, and the bottom graph shows the frequency response of the sound pressure.

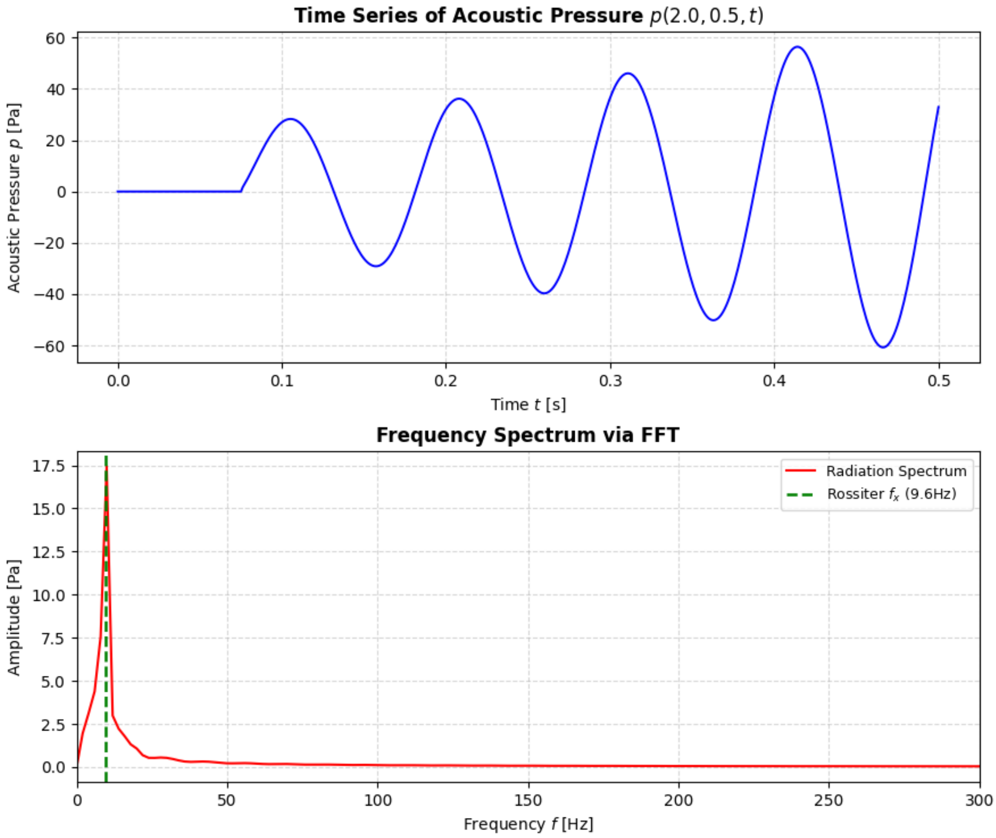

Fig. 3 Numerical Calculation Result ($(x, y) = (2.0, 0.5)$)

Looking at the top graph in Fig. 3, we can see that time is required for the sound to travel from the sound source. Also, from the frequency response below, a peak at 9.6 (Hz) appears, corresponding to the first frequency of Rossiter formula f_x. That is, for $x \geq L_H$, the sound has frequency components consisting only of the first frequency of Rossiter formula f_x, which is the frequency of forced oscillation.

Next, Fig. 4 shows the numerical calculation results for $U = 1133.3$ (m/s), with the observation point set at $(x, y) = (0.01, 0.01)$ near the origin. It can be seen that the first-order resonance frequencies of f_x and f_{xr} coincide, resulting in the generation of a very loud sound. In other words, a lock-in phenomenon is occurring.

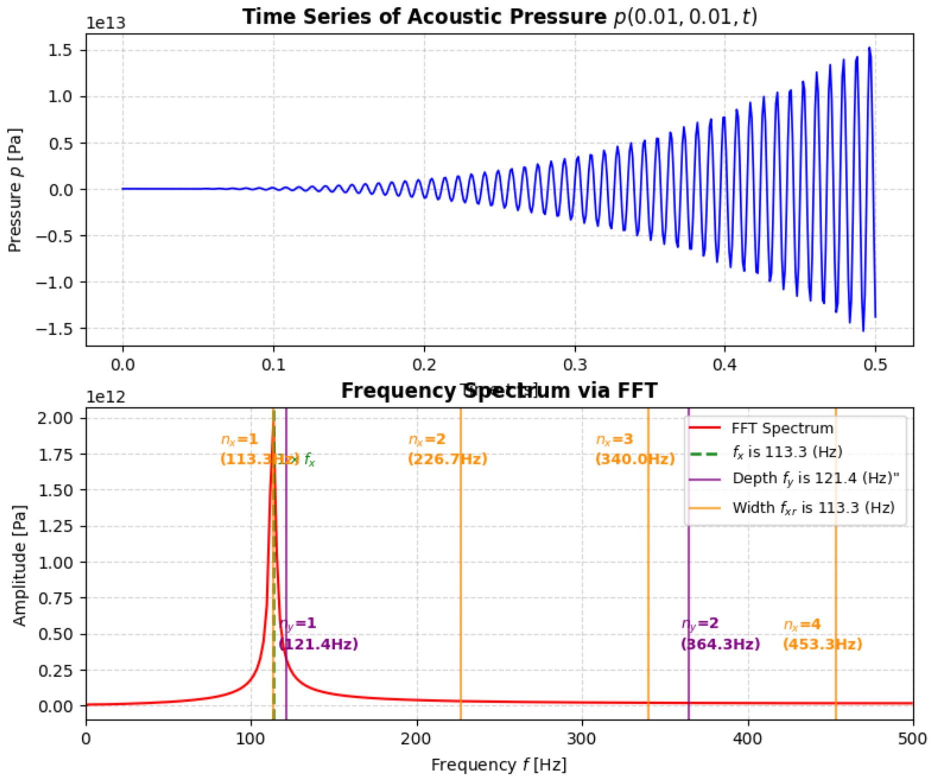

Fig. 4 Numerical Calculation Result (U = 1133.3(m/s))

Next, Fig. 5 shows the numerical calculation results for $U = 1700.0$ (m/s), with the observation point set at $(x, y) = (0.01, 0.01)$ near the origin. It can be seen that the first-order resonant frequencies of f_x and f_{xr} are present. Furthermore, small peaks are also observed at the second and third orders of resonance in the x-direction. This supports the discussion regarding Equation (26).

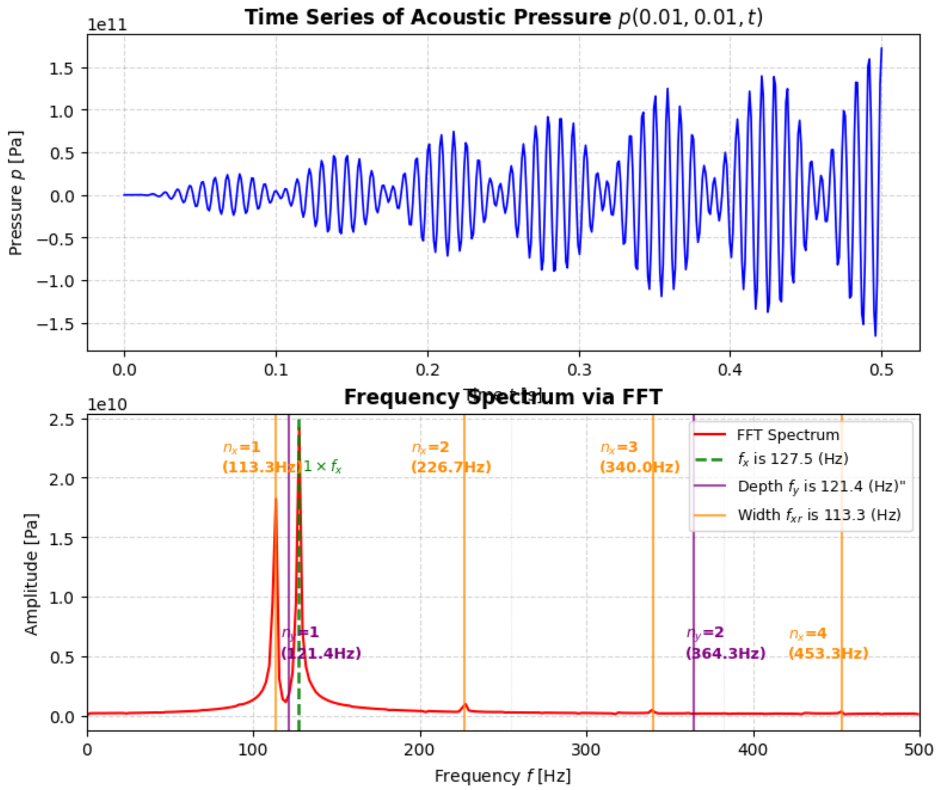

Fig. 5 Numerical Calculation Result (U = 1700.0(m/s))

Finally, Fig. 6 shows the numerical calculation results for $U = 1415.5$ (m/s), with the observation point set at $(x, y) = (0.01, 0.01)$ near the origin. The first-order resonance frequency of f_x is present at the same magnitude as the first-order resonance frequency of f_y, and a peak appears at that frequency. However, no peak appears at the second-order resonance frequency of f_y Therefore, it is considered that the resonance sound of f_x is being produced, rather than the resonance in the y-direction being excited. Conversely, regarding resonance in the x-direction, small peaks are present even at the second and third orders. This corroborates the discussion concerning Equation (26).

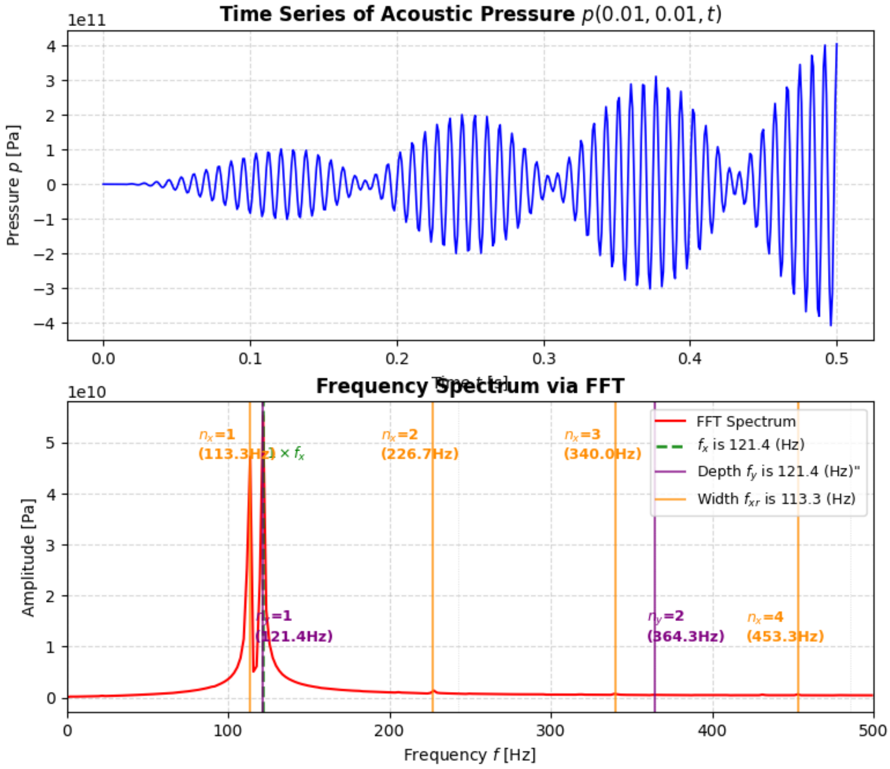

Fig. 6 Numerical Calculation Result (U = 1415.5(m/s))

5. Conclusion

Research on automobile whistling and suction sounds has been conducted in the past. For cavity resonance, a type of whistling sound, the cavity resonance frequency has been determined using Rossiter's empirical formula. Therefore, we limited our study to the two-dimensional case and clarified the physical phenomena that arise by solving a set of partial differential equations that explain the phenomenon. As a result, the horizontal resonance frequency was found to become proportional to the speed of sound as the mainstream velocity increased, and the resonance frequency of the cavity space was also determined. Finally, we discussed the conditions under which resonance increases. Finally, we were able to confirm the conditions under which resonance increases through numerical calculations.

References

Calvo, J. A., Diaz, V., & San Roman, J. L. (2005). *Controlling the turbocharger whistling* *noise in diesel engines.* International Journal of Vehicle Noise and Vibration, Vol. 2, No. 1. doi:https://doi.org/10.1504/IJVNV.2006.008524

Chien-Hsiung, T., Lung-Ming , F., Chang-Hsien , T., Yen-Loung , H., & Jik-Chang , L. (2009). *Computational aero-acoustic analysis of a passenger car with a rear spoiler.* Applied Mathematical Modelling, Volume 33, Issue 9. doi:https://doi.org/10.1016/j.apm.2008.12.004

George, A. R. (1990). *Automobile Aerodynamic Noise.* SAE Transactions, Vol. 99, Section 6. Retrieved from http://www.jstor.org/stable/44553993

Jagtiani, H. (1972). *The Objective Method of Evaluating Aspiration Wind Noise.* SAE Technical Paper 720506. doi:https://doi.org/10.4271/720506

Jung, W., & Oh, S. (1995). *The Influence of Vehicle Elements to Aspiration Wind Noise.* SAE Technical Paper 950624. doi:https://doi.org/10.4271/950624

Münder, M., & Carbon, C.-C. (2022). *Howl, whirr, and whistle: The perception of electric powertrain noise and its importance for perceived quality in electrified vehicles.* Applied Acoustics, Volume 185. doi:https://doi.org/10.1016/j.apacoust.2021.108412

Oettle, N., & Sims-Williams, D. (2017). *Automotive aeroacoustics: An overview.* Journal of Automobile Engineering, Volume 231, Issue 9. doi:https://doi.org/10.1177/0954407017695147

Qatu, M. S., Abdelhamid, M. K., Pang, J., & Sheng, G. (2009). *Overview of automotive noise and vibration.* International Journal of Vehicle Noise and Vibration, Vol. 5, No. 1-2. doi:https://doi.org/10.1504/IJVNV.2009.029187

Wang, Q., Chen, X., & Zhang, Y. (2021). *An Overview of Automotive Wind Noise and Buffeting Active Control.* SAE International Journal of Vehicle Dynamics, Stability, and NVH, 5(4). doi:https://doi.org/10.4271/10-05-04-0030

Zhang, F., Meng, W., Li, X., & Zheng, C. (2022). *A vehicle whistle database for evaluation of outdoor acoustic source localization and tracking using an intermediate-sized microphone array.* Applied Acoustics, Volume 201. doi:https://doi.org/10.1016/j.apacoust.2022.109113